

Topological Semimetals carrying Arbitrary Hopf Numbers: Hopf-Link, Solomon's-Knot, Trefoil-Knot and Other Semimetals

Motohiko Ezawa

Department of Applied Physics, University of Tokyo, Hongo 7-3-1, 113-8656, Japan

We propose a new type of Hopf semimetals indexed by a pair of numbers (p, q) , where the Hopf number is given by pq . The Fermi surface is given by the preimage of the Hopf map, which consists of loops nontrivially linked for a nonzero Hopf number. The Fermi surface forms a torus link, whose examples are the Hopf link indexed by $(1, 1)$, the Solomon's knot $(2, 1)$, the double Hopf-link $(2, 2)$ and the double trefoil-knot $(3, 2)$. We may choose p or q to be a half integer, where the Fermi surface is a torus knot such as the trefoil knot $(3/2, 1)$. It is even possible to make the Hopf number an arbitrary rational number, where a semimetal whose Fermi surface forms open strings is generated.

Introduction: Weyl semimetals are described by the two-band model equipped with a point node in the three-dimensional (3D) space^{1,2}. It is characterized by the monopole charge in the momentum space³. Line-nodal semimetals or loop-nodal semimetals are also possible in the 3D space, where the zero-energy Fermi surface is given by a line or a closed loop⁵⁻¹⁵. Recently, a nodal-chain semimetal is proposed, where loop nodes touch with each other⁴. A natural question is whether nontrivial Fermi-surfaces made of loop nodes such as links and knots are possible.

The two-band Hamiltonian $H = \mathbf{S}(\mathbf{k}) \cdot \boldsymbol{\sigma}$ is a prototype of Hopf insulators¹⁶⁻²¹, where $\boldsymbol{\sigma} = (\sigma_x, \sigma_y, \sigma_z)$ are the Pauli matrices and $\mathbf{S}(\mathbf{k})$ is the normalized pseudospin $|\mathbf{S}(\mathbf{k})| = 1$ spanning the sphere surface \mathbb{S}^2 . On the other hand, the 3D Brillouin zone is identical to the torus \mathbb{T}^3 . A homotopy from \mathbb{T}^3 to \mathbb{S}^2 is characterized by the Hopf number. It has been argued that Hopf insulators with arbitrary Hopf numbers are possible¹⁷. Nontrivial Hopf textures are also discussed in cold atoms^{22,23}, light fields²⁴ and liquid crystal²⁵.

In this Letter we investigate topological semimetals, where Fermi surfaces consist of nontrivial loops with arbitrary Hopf numbers. We explore the Hamiltonian $H = S_x \sigma_x + S_z \sigma_z$, where the zero-energy condition reads $S_y = \pm 1$. The Fermi surface is the preimage of the points $\mathbf{S}_{\pm} = (0, \pm 1, 0)$ in the mapping $\mathbb{T}^3 \rightarrow \mathbb{S}^2$, and it consists of two loops. They are linked for a nonzero Hopf number. We construct Fermi surfaces comprised of the Hopf link, the Solomon's knot and others: See Fig.1. They are "torus links" lying on the surface of a torus. Furthermore, we construct Fermi surfaces comprised of torus knots by choosing half integer Hopf numbers, among which there arises in particular a trefoil-node Fermi surface. We can even choose any one rational number as a Hopf number, where the Fermi surface forms open strings though it describes no longer a topological semimetal.

Torus-link semimetals: The Hamiltonian of topological Hopf insulators is given by¹⁶⁻²¹

$$H(\mathbf{k}) = \mathbf{S}(\mathbf{k}) \cdot \boldsymbol{\sigma}, \quad (1)$$

where $\mathbf{S}(\mathbf{k})$ is the normalized pseudospin field, $|\mathbf{S}(\mathbf{k})| = 1$. It is written as $\mathbf{S} = \mathbf{z}^\dagger \boldsymbol{\sigma} \mathbf{z}$ in terms of the $\mathbb{C}\mathbb{P}^1$ field \mathbf{z} . We define it by

$$\mathbf{z} \equiv \begin{pmatrix} z_\uparrow \\ z_\downarrow \end{pmatrix} = \frac{1}{\sqrt{|\eta_\uparrow|^{2p} + |\eta_\downarrow|^{2q}}} \begin{pmatrix} \eta_\uparrow^p \\ \eta_\downarrow^q \end{pmatrix}, \quad (2)$$

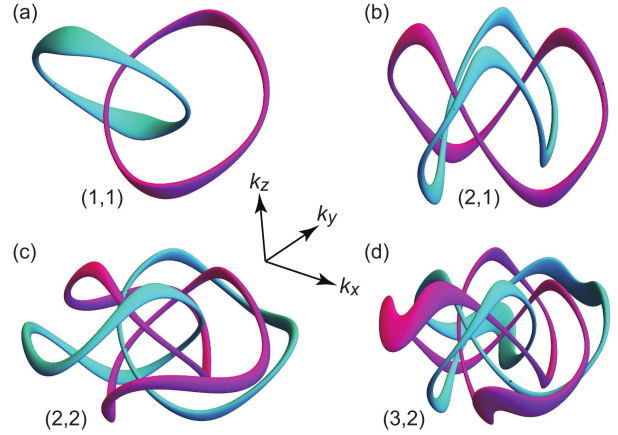


FIG. 1: Bird's eye's view of the almost zero-energy surface of the Hamiltonian H_{xz} . (a) The Hopf-link semimetal with $(p, q) = (1, 1)$, (b) the Solomon's-knot semimetal with $(2, 1)$, (c) the double Hopf-link semimetal with $(2, 2)$, which consists of two Hopf links. (d) the double trefoil-knot semimetal with $(3, 2)$. We have chosen $m = 2$ in Eq.(3) to draw figures. The preimage of $S_y = 1$ is colored in magenta, while that of $S_y = -1$ is colored in cyan.

where η_\uparrow and η_\downarrow are complex numbers given by¹⁶⁻²⁰

$$\begin{aligned} \eta_\uparrow(\mathbf{k}) &= \sin k_x + i \sin k_y, \\ \eta_\downarrow(\mathbf{k}) &= \sin k_z + i(\cos k_x + \cos k_y + \cos k_z - m), \end{aligned} \quad (3)$$

while p and q are integers. We note that p and q are originally introduced as a set of coprime integer¹⁷ but here we do not impose it. We will see that p and q can be generalized even to rational numbers though a cut is introduced. The normalized pseudospin is explicitly represented as

$$S_x + iS_y = \frac{2\eta_\uparrow^p \eta_\downarrow^q}{|\eta_\uparrow|^{2p} + |\eta_\downarrow|^{2q}}, \quad S_z = \frac{|\eta_\uparrow|^{2p} - |\eta_\downarrow|^{2q}}{|\eta_\uparrow|^{2p} + |\eta_\downarrow|^{2q}}. \quad (4)$$

We consider a class of pseudospin textures indexed by a pair of numbers (p, q) in the Hamiltonian (1).

The $\mathbb{C}\mathbb{P}^1$ field takes values on the 3D sphere \mathbb{S}^3 since it contains four real numbers, $N_1 = \text{Re } z_\uparrow(\mathbf{k})$, $N_2 = \text{Im } z_\uparrow(\mathbf{k})$, $N_3 = \text{Re } z_\downarrow(\mathbf{k})$ and $N_4 = \text{Im } z_\downarrow(\mathbf{k})$, together with the normalization condition $\sum_i N_i^2 = 1$. It gives a mapping $\mathbb{T}^3 \rightarrow \mathbb{S}^3$, for the Brillouin zone is a 3D torus. On the other

hand, the normalized pseudospin expressed as $\mathbf{S} = \mathbf{z}^\dagger \sigma \mathbf{z}$ defines a mapping $\mathbb{S}^3 \rightarrow \mathbb{S}^2$, for it takes values on the sphere \mathbb{S}^2 . Consequently the underlying structure of the Hamiltonian (1) is a mapping $\mathbb{T}^3 \rightarrow \mathbb{S}^3 \rightarrow \mathbb{S}^2$ from the Brillouin zone to the pseudospin space.

The combined mapping $\mathbb{T}^3 \rightarrow \mathbb{S}^2$ is indexed by the Hopf number¹⁶⁻²¹

$$\Gamma(p, q) = -\frac{1}{2\pi^2} \int_{\text{BZ}} d\mathbf{k} \varepsilon_{\mu\nu\rho\tau} N_\mu \partial_{k_x} N_\nu \partial_{k_y} N_\rho \partial_{k_z} N_\tau. \quad (5)$$

By inserting (3) to this formula we obtain

$$\Gamma(p, q) = \begin{cases} 0, & |m| > 3 \\ pq, & 1 < |m| < 3 \\ -2pq, & |m| < 1 \end{cases}. \quad (6)$$

We note that the definition of the Hopf number (5) is different from the previous literature¹⁷, in which it is defined in terms of $(\eta_\uparrow, \eta_\downarrow)$ rather than $(z_\uparrow, z_\downarrow)$. The formula (6) is understood intuitively as follows: When $p = q = 1$, it is a well-known formula for the Hopf number¹⁷, which indicates that there exist one circle in the interior of the torus and one circle around its axis of rotational symmetry. Now, $z_\uparrow \propto \eta_\uparrow^p$ and $z_\downarrow \propto \eta_\downarrow^p$ imply that there exist p and q of these circles.

The energy spectrum of the Hamiltonian (1) reads $E(\mathbf{k}) = \pm \sqrt{S_x^2(\mathbf{k}) + S_y^2(\mathbf{k}) + S_z^2(\mathbf{k})}$. The Fermi surface of the topological Hopf insulator is constructed by the intersection of the three curved surfaces, $S_x = S_y = S_z = 0$. In general, the intersection of three surfaces is null, which results in an insulating state.

In order to construct a model having a Fermi surface, it is necessary to reduce the number of the conditions on the zero-energy states. There exist three trivial ways to do so. We may employ any one of the conditions, $S_x = S_z = 0$, $S_y = S_z = 0$, or $S_x = S_y = 0$. Obviously, they are the zero-energy conditions of the following three Hamiltonians,

$$H_{xz}(\mathbf{k}) = S_x(\mathbf{k}) \sigma_x + S_z(\mathbf{k}) \sigma_z, \quad (7)$$

$$H_{yz}(\mathbf{k}) = S_y(\mathbf{k}) \sigma_y + S_z(\mathbf{k}) \sigma_z, \quad (8)$$

$$H_{xy}(\mathbf{k}) = S_x(\mathbf{k}) \sigma_x + S_y(\mathbf{k}) \sigma_y, \quad (9)$$

respectively. The Fermi surface constructed by the intersection of the two curved surfaces is a line node in general. In all these models we use the same CP^1 field (2) to define $S_i(\mathbf{k})$. Only the Hamiltonian H_{xz} preserves the combination symmetry PT of the time reversal T and inversion symmetry P .

The H_{xz} model: We first investigate the Hamiltonian H_{xz} . From the normalization condition on $\mathbf{S}(\mathbf{k})$, the zero-energy condition is expressed as $S_y(\mathbf{k}) = \pm 1$. Namely, the Fermi surface is the preimage of the points $\mathbf{S}_\pm = (0, \pm 1, 0)$ in the combined Hopf map $\mathbb{T}^3 \rightarrow \mathbb{S}^2$, which is a circle \mathbb{S}^1 in the 3D Brillouin zone. Consequently there are at least two loops corresponding to the preimage of $S_y(\mathbf{k}) = 1$ and $S_y(\mathbf{k}) = -1$ in the 3D Brillouin zone. These two loops form a link when the Hopf number is nonzero.

Various links indexed by a pair (p, q) are realized in the 3D Brillouin zone. We show an almost zero-energy surface $E = \delta$ with $|\delta| \ll 1$ for (p, q) in Figs.1 and 2. The

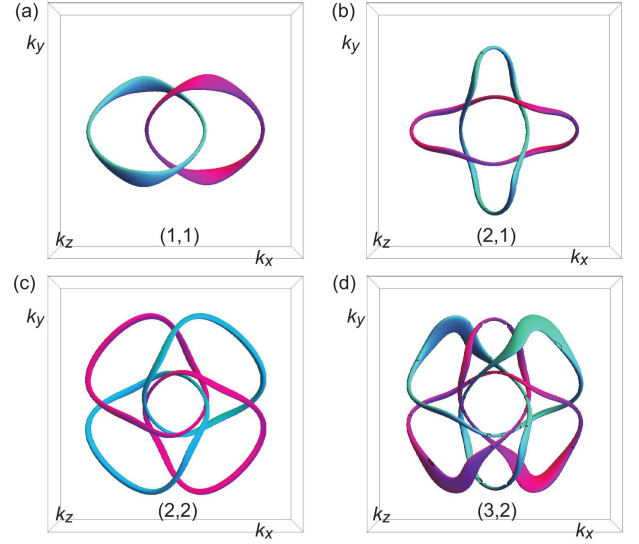


FIG. 2: Top view of almost zero-energy surface of the Hamiltonian H_{xz} in the 3D Brillouin zone. See the caption of Fig.1 for (a)~(d).

preimage of $S_y(\mathbf{k}) = 1$ is colored in magenta and that of $S_y(\mathbf{k}) = -1$ is colored in cyan. For example, the Hopf link and the Solomon's knot are realized by taking pairs (1, 1) and (2, 1), respectively. The Fermi surface for (3, 2) is given by the combination of two trefoils, which we call a double trefoil.

We recall the terminology in the link theory. A link lying on the surface of a torus is called a torus link. The torus link $T(p, q)$ winds q times around a circle in the interior of the torus, and p times around its axis of the rotational symmetry. In the present context, the surface determined by the condition $S_z = 0$ gives a torus. Thus the node indexed by (p, q) is the torus link $T(2p, 2q)$, where the factor 2 appears because it is the preimage of the two points $S_\pm = (0, \pm 1, 0)$. According to the link theory, $T(2p, 2q)$ is identical to $T(2q, 2p)$. Furthermore, $T(-2p, 2q)$ link and $T(2p, -2q)$ are mirror images of $T(2p, 2q)$.

If p and q are not relatively prime, we have a torus link with more than one component. The number of the loops is given by $\text{gcd}(2p, 2q) = 2\text{gcd}(p, q)$, where gcd represents the greatest common divisor. For example, the Fermi surface consists of four loop nodes for $p = 2$ and $q = 2$. This looks a bit odd since we have discussed that two loops arise as the preimage of $S_y = \pm 1$. It is an interesting problem how such a Fermi surface consisting more than two loops is realized for $\text{gcd}(p, q) \neq 1$. We assume $\text{gcd}(p, q) = s$. Then we can write $p = sp'$ and $q = sq'$, where p' and q' are coprime integers. The solutions are given by $\eta_\uparrow^{1/s}$ and $\eta_\downarrow^{1/s}$, where η_\uparrow and η_\downarrow satisfy the $S_y = \pm 1$ for the model with p' and q' . The roots of $\eta_\uparrow^{1/s}$ and $\eta_\downarrow^{1/s}$ have s solutions, which results in the s Fermi loops.

In the following, we derive the equations to determine the link. The zero-energy states must satisfy the condition $S_z = \mathbf{z}^\dagger \sigma_z \mathbf{z} = |z_\uparrow|^2 - |z_\downarrow|^2 = 0$. By combining it with the normalization condition $|z_\uparrow|^2 + |z_\downarrow|^2 = 1$, the CP^1 field is

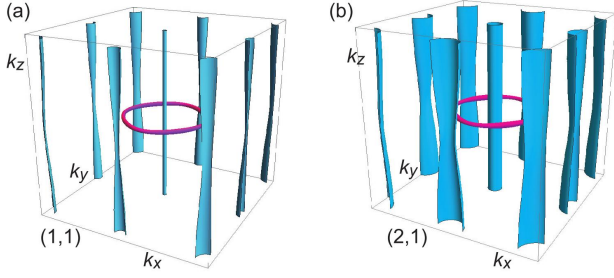


FIG. 3: Bird's eye's view of the almost zero-energy surface of the Hamiltonian H_{xy} for (a) the pair $(p, q) = (1, 1)$ and (b) $(2, 1)$.

parametrized as

$$z_{\uparrow} = \frac{1}{\sqrt{2}} e^{i\theta_{\uparrow}}, \quad z_{\downarrow} = \frac{1}{\sqrt{2}} e^{i\theta_{\downarrow}}. \quad (10)$$

The zero-energy states correspond to $S_y = \pm 1$, which reads

$$S_y = \mathbf{z}^{\dagger} \sigma_y \mathbf{z} = -\sin(\theta_{\uparrow} - \theta_{\downarrow}) = \pm 1.$$

The solution is given by $\theta_{\uparrow} - \theta_{\downarrow} = \mp \frac{\pi}{2}$. We find the relation $z_{\downarrow} = \pm i z_{\uparrow}$, or

$$\eta_{\downarrow}^q = \pm i \eta_{\uparrow}^p. \quad (11)$$

These two equations determine the Fermi surface made of links.

The H_{yz} model: The Fermi surface of H_{yz} is topologically equivalent to that of H_{xz} model. The only difference is that the Fermi surface is rotated 90 degree between the H_{xz} and H_{yz} models.

The H_{xy} model: The Fermi surface of H_{xy} looks very different, where some of the Fermi surfaces form lines penetrating the whole Brillouin zone: See Fig.3. The model H_{xy} is instructive since we obtain various analytical expressions.

The zero-energy condition in the model H_{xy} is given by the preimage of $S_z = |z_{\uparrow}|^2 - |z_{\downarrow}|^2 = \pm 1$. By combining it with the normalization condition $|z_{\uparrow}|^2 + |z_{\downarrow}|^2 = 1$, the preimage of $S_z = 1$ is given by $|z_{\uparrow}|^2 = 1$ and $|z_{\downarrow}|^2 = 0$, which is equivalent to the condition $|z_{\downarrow}|^2 = |\eta_{\downarrow}|^{2q} = 0$, where

$$|\eta_{\downarrow}|^2 = \sin^2 k_z + (\cos k_x + \cos k_y + \cos k_z - m)^2 = 0. \quad (12)$$

The solution is

$$\cos k_x + \cos k_y = m - 1, \quad k_z = 0, \quad (13)$$

which represents q -fold degenerate loop nodes.

On the other hand, the preimage of $S_z = -1$ is given by $|z_{\uparrow}|^2 = 0$ and $|z_{\downarrow}|^2 = 1$, which is equivalent to the condition $|z_{\uparrow}|^2 = |\eta_{\uparrow}|^{2p} = 0$, where

$$|\eta_{\uparrow}|^2 = \sin^2 k_x + \sin^2 k_y = 0.$$

The solution represents p -fold degenerate line nodes along the k_z direction described by $k_x = n_x \pi$, $k_y = n_y \pi$, k_z with $-\pi \leq k_z \leq \pi$, where n_x and n_y are integers.

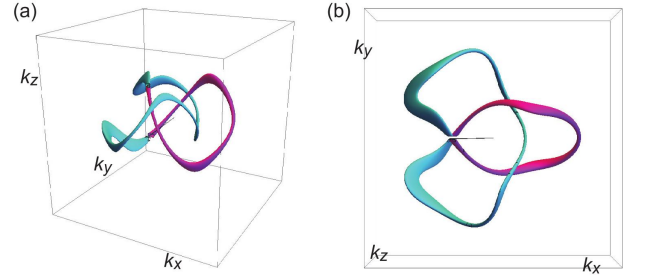


FIG. 4: Trefoil-knot semimetal with $p = 3/2$ and $q = 1$. (a) Bird's eye's view and (b) the top view of the almost zero-energy surface. There is a cut on the $k_y = 0$ plane for $k_x < 0$, where the magenta and cyan curves touch.

We may also analyze this Hamiltonian system from the view point of the Berry curvature. We introduce a continuum model defined by

$$\begin{aligned} \eta_{\uparrow}(\mathbf{k}) &= k_x + i k_y, \\ \eta_{\downarrow}(\mathbf{k}) &= k_z + i(3 - m - (k_x^2 + k_y^2 + k_z^2)/2). \end{aligned} \quad (14)$$

The Fermi surface is topologically equivalent to the original model (3). The only difference is the approximation of the loop (13) by the circle $k_x^2 + k_y^2 = 2(3 - m)$, which does not change the linking structure.

By using them we may derive explicitly the eigenstate $|\psi\rangle$ of the Hamiltonian (9). The Berry connection $A_{k_i} = -i \langle \psi | \partial_{k_i} | \psi \rangle$ is given by

$$A_k = \frac{2kqk_z}{k_z^4 + k_z^2(k^2 + 2m - 4) + (k^2 + 2m - 6)^2}, \quad (15)$$

$$A_{\theta} = \frac{p}{2}, \quad (16)$$

$$A_z = \frac{q(k_z^2 - k^2 - 2m + 6)}{k_z^4 + k_z^2(k^2 + 2m - 4) + (k^2 + 2m - 6)^2}, \quad (17)$$

where we have introduced the polar coordinate $k_x = k \cos \theta$ and $k_y = k \sin \theta$. We show the Berry curvature in Fig.5. We find a vortex structure along a line node (cyan line in Fig.3) described by $k_x = 0$, $k_y = 0$, k_z with $-\pi \leq k_z \leq \pi$, and a circle described by $k_x^2 + k_y^2 = 6 - 2m$, $k_z = 0$. Actually this line node has a p -fold degeneracy. Indeed, we calculate the Berry phase along a loop encircling the line node to find that

$$\Gamma_B = \oint A_i dk_i = \int_0^{2\pi} A_{\theta} d\theta = p\pi, \quad (18)$$

which is quantized and represents the degeneracy. In the same way, the Berry phase along a small circle around a loop node (magenta loop in Fig.3) is obtained as

$$\Gamma_B = \oint A_i dk_i = \int_0^{2\pi} A_{\theta} d\theta = q\pi, \quad (19)$$

representing the degeneracy of the loop node. Thus the indices p and q are detected separately, while only the product pq appears in the Hopf number.

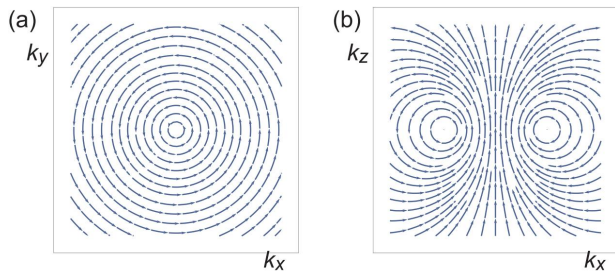


FIG. 5: (a) Stream plot of the Berry curvature (A_x, A_y) along the k_x - k_y plane with $k_z = 0$ and (b) Stream plot of the Berry curvature (A_x, A_z) on the k_x - k_z plane at $k_y = 0$.

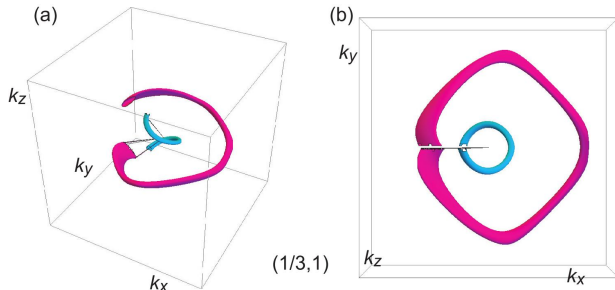


FIG. 6: Open-string semimetal with $p = 1/3$ and $q = 1$. (a) Bird's eye's view and (b) top view of almost zero-energy surface. There is a cut along the $k_y = 0$ plane for $k_x < 0$, where the ends of the open string exist.

Torus-knot semimetals: We have seen that the Fermi surfaces consist of at least two loops, which form a torus link. It is an interesting problem whether we can construct a Fermi surface consist of one nontrivial loop, which is a torus knot. Since the number of loops is given by $2\text{gcd}(p, q)$, we must take one of p and q non-integer. We find that a torus-knot Fermi surface is realized by taking a half-integer p . For example, we can realize a trefoil Fermi surface by taking $p = 3/2$ and $q = 1$, which is shown in Fig.4. There is a cut in the momentum space due to the square root contribution in the Hamiltonian. Namely, only the magenta or cyan curve does not form a closed loop but form a loop with the combination of them.

Open string semimetals: It is possible to choose even any rational numbers for p or q , which creates an open string Fermi surface as shown in Fig.6. This is understood as follows. The model with p and q gives the torus link $T(2p, 2q)$. If one of the p and q is not a half integer, it cannot describe a closed loop, generating to an open string. The ends of the open string are on the cut plane.

The author is very much grateful to N. Nagaosa for many helpful discussions on the subject. This work is supported by the Grants-in-Aid for Scientific Research from MEXT KAKENHI (Grant Nos.JP17K05490 and 15H05854).

Note added: During the preparation of this manuscript, we became aware of closely related works²⁶⁻²⁸, where various linked nodal semimetals are proposed. Especially, this work has turned out to be a generalization of the work²⁷, where only the case with $p = q = 1$ is studied.

- ¹ P. Hosur, X.L. Qi, C. R. Physique 14, 857 (2013).
- ² S. Jia, S.-Y. Xu, M. Z. Hasan, Nature Materials 15, 1140 (2016).
- ³ S. Murakami, New J. Phys. 9, 356 (2007).
- ⁴ T. Bzduck, Q.-S. Wu, A. Ruegg, M. Sigrist and A. A. Soluyanov, Nature 538, 75 (2016).
- ⁵ S. Mandal and N. Surendran Phys. Rev. B 79, 024426 (2009).
- ⁶ A. A. Burkov, M. D. Hook, and L. Balents, Phys. Rev. B 84, 235126 (2011).
- ⁷ M. Phillips and V. Aji, Phys. Rev. B 90, 115111 (2014).
- ⁸ C. Fang, Y. Chen, H.-Y. Kee and L. Fu, Phys. Rev. B 92, 081201 (2015).
- ⁹ L. S. Xie, L. M. Schoop, E. M. Seibel, Q. D. Gibson, W. Xie, and R. J. Cava, APL Materials 3, 083602 (2015).
- ¹⁰ R. Yu, H. Weng, Z. Fang, X. Dai and X. Hu, Phys. Rev. Lett. 115, 036807 (2015).
- ¹¹ Y. Kim, B. J. Wieder, C. L. Kane, and A. M. Rappe, Phys. Rev. Lett. 115, 036806 (2015).
- ¹² A. Yamakage, Y. Yamakawa, Y. Tanaka, Y. Okamoto, J. Phys. Soc. Jpn. 85, 013708 (2016).
- ¹³ M. Ezawa, Phys. Rev. Lett. Phys. Rev. Lett. 116, 127202 (2016).
- ¹⁴ M. Hirayama, R. Okugawa, T. Miyake, and S. Murakami, Nat. Com. 8, 14022 (2017).
- ¹⁵ Y.-H. Chan, C.-K. Chiu, M. Y. Chou, and A. P. Schnyder, Phys. Rev. B 93, 205132 (2016).
- ¹⁶ J. E. Moore, Y. Ran and X.-G. Wen, Phys. Rev. Lett. 101, 186805 (2008).
- ¹⁷ D.-L. Deng, S.-T. Wang, C. Shen, and L.-M. Duan, Phys. Rev. B 88, 201105(R) (2013).
- ¹⁸ D.-L. Deng, S.-T. Wang, and L.-M. Duan, Phys. Rev. B 89, 075126 (2014).
- ¹⁹ D.-L. Deng, S.-T. Wang, K. Sun, and L.-M. Duan, cond-mat/arXiv:1612.01518.
- ²⁰ R. Kennedy, Phys. Rev. B 94, 035137 (2016).
- ²¹ C. Liu, F. Vafa and C. Xu cond-mat/arXiv:1612.04905.
- ²² Y. Kawaguchi, M. Nitta, and M. Ueda, Phys. Rev. Lett. 100, 180403 (2008).
- ²³ D. S. Hall, M. W. Ray, K. Tiurev, E. Ruokokoski, A. H. Gheorghe and M. Mottonen, Nat. Phys. 12, 478 (2016).
- ²⁴ H. Kedia, I. Bialynicki-Birula, D. Peralta-Salas, and W. T. M. Irvine, Phys. Rev. Lett. 111, 150404 (2013).
- ²⁵ P. J. Ackerman and I. I. Smalyukh, Phys. Rev. X 7, 011006 (2017).
- ²⁶ W. Chen, H.-Z. Lu, and J.-M. Hou, cond-mat/arXiv:1703.10886.
- ²⁷ Z. Yan, R. Bi, H. Shen, L. Lu, S.-C. Zhang, and Z. Wang, cond-mat/arXiv:1704.00655.
- ²⁸ P.-Y. Chang and C.-H. Yee, cond-mat/arXiv:1704.01948.